

A Local, Interactive Network of 3' RNA Elements Supports Translation and Replication of Turnip Crinkle Virus

Xuefeng Yuan, Kerong Shi and Anne E. Simon
J. Virol. 2012, 86(8):4065. DOI: 10.1128/JVI.07019-11.
Published Ahead of Print 15 February 2012.

Updated information and services can be found at:
<http://jvi.asm.org/content/86/8/4065>

	<i>These include:</i>
REFERENCES	This article cites 44 articles, 24 of which can be accessed free at: http://jvi.asm.org/content/86/8/4065#ref-list-1
CONTENT ALERTS	Receive: RSS Feeds, eTOCs, free email alerts (when new articles cite this article), more»

Information about commercial reprint orders: <http://jvi.asm.org/site/misc/reprints.xhtml>
To subscribe to to another ASM Journal go to: <http://journals.asm.org/site/subscriptions/>

A Local, Interactive Network of 3' RNA Elements Supports Translation and Replication of Turnip Crinkle Virus

Xuefeng Yuan,* Kerong Shi,* and Anne E. Simon

Department of Cell Biology and Molecular Genetics, University of Maryland College Park, College Park, Maryland, USA

The majority of the 3' untranslated region (UTR) of *Turnip crinkle virus* (TCV) was previously identified as forming a highly interactive structure with a ribosome-binding tRNA-shaped structure (TSS) acting as a scaffold and undergoing a widespread conformational shift upon binding to RNA-dependent RNA polymerase (RdRp). Tertiary interactions in the region were explored by identifying two highly detrimental mutations within and adjacent to a hairpin H4 upstream of the TSS that reduce translation *in vivo* and cause identical structural changes in the loop of the 3' terminal hairpin Pr. Second-site changes that compensate for defects in translation/accumulation and reverse the structural differences in the Pr loop were found in the Pr stem, as well as in a specific stem within the TSS and within the capsid protein (CP) coding region, suggesting that the second-site changes were correcting a conformational defect and not restoring specific base pairing. The RdRp-mediated conformational shift extended upstream through this CP open reading frame (ORF) region after bypassing much of an intervening, largely unstructured region, supporting a connection between 3' elements and coding region elements. These data suggest that the Pr loop, TSS, and H4 are central elements in the regulation of translation and replication in TCV and allow for development of an RNA interactome that maps the higher-order structure of a postulated RNA domain within the 3' region of a plus-strand RNA virus.

The genomes of positive-strand RNA viruses control fundamental processes such as translation and replication through multiple RNA elements that interact dynamically with each other and with viral and host proteins. Upon entry into host cells, the viral genomic RNA (gRNA) is recognized as a template by the host translational apparatus for production of replication-associated proteins, which combine with an increasingly diverse variety of host factors to synthesize negative-strand RNAs that then serve as the templates for synthesis of progeny positive-strand RNAs (1, 7, 8, 19). The widespread positioning of *cis*-elements that function in translation and/or replication requires short-range or long-range bridges within the RNA to deliver bound elements to locations where the specific processes initiate.

Understanding how functional, dynamic RNA structures regulate viral processes requires a detailed knowledge of the topology of important regions of the RNA genome and the canonical and noncanonical tertiary interactions that connect various elements. Attempts to decipher networks of short- and long-distance RNA-RNA interactions have been limited to a few viruses. For dengue virus (DENV), several sets of overlapping 5'- and 3'-interacting sequences have been identified that control the balance between linear and circular forms of the genome, which is critical for replication but not translation (13, 38). *Tomato bushy stunt virus* (TBSV) requires a complex network of long-distance RNA-RNA interactions to promote replication, subgenomic RNA (sgRNA) synthesis, translation initiation, and translational recoding (4, 14, 20, 40). For both examples, however, only canonical Watson-Crick interactions have been elucidated.

Tertiary interactions that comprise major components of an RNA landscape include significant levels of noncanonical base pairing, with estimations that up to 96% of residues in an RNA participate in local or distal base pairs using all three edges of the base (i.e., Watson-Crick, Hoogsteen, or Sugar) (17, 32). In the absence of nuclear magnetic resonance (NMR) or X-ray crystallography data, noncanonical interactions can be detected using (i) RNA structure assays that report on changes in the flexibility or

pairing status of residues or (ii) genetic selection, which makes use of the error-prone nature of RNA-dependent RNA polymerase (RdRp) to generate second-site mutations that compensate for deleterious primary mutations. Once noncanonical interactions are suspected, covariation analysis can confirm specific interactions, since base substitutions that maintain isostericity of noncanonical base pairs are favored during natural selection (17, 18, 47). Despite the availability of these approaches, maps delineating tertiary interactions in regions of moderate length have not been produced for any viral RNA.

Turnip crinkle virus (TCV), a member of the *Carmovirus* genus in the *Tombusviridae*, has a limited genome size (4,054 nucleotides [nt]) and coding capacity (five proteins), allowing it to serve as an excellent model for studies on RNA structure/function (24) (Fig. 1A). Based on genetic covariation, biochemical structure assays, and phylogenetic comparisons between related carmoviruses, the 3' untranslated region (UTR) of TCV is known to contain five hairpins (H4, H4a, H4b, H5, and Pr), four canonically base-paired pseudoknots (Ψ_1 , Ψ_2 , Ψ_3 , Ψ_4), and a largely unstructured region (USR) that begins just upstream of the capsid protein (CP) termination codon and extends to near the base of hairpin H4 (Fig. 1B) (22, 35). The 3' proximal Pr hairpin, which is structurally conserved in all carmoviruses, serves as the core promoter for minus-strand synthesis in TCV-associated, sequence-related satellite

Received 6 December 2011 Accepted 2 February 2012

Published ahead of print 15 February 2012

Address correspondence to Anne E. Simon, simona@umd.edu.

* Present address: X. Yuan, College of Plant Protection, Shandong Agricultural University, Taian, Shandong Province, People's Republic of China; K. Shi, College of Animal Science and Veterinary Medicine, Shandong Agricultural University, Taian, Shandong Province, People's Republic of China.

Copyright © 2012, American Society for Microbiology. All Rights Reserved.

doi:10.1128/JVI.07019-11

RNA *satC* and is important for replication in TCV (30, 37, 43). In addition, the Pr hairpin terminal loop was recently found to engage in a long-distance interaction that enhances ribosomal read-through, leading to the synthesis of the p88 RdRp (4). Hairpins H4a, H4b, and H5, along with pseudoknots Ψ_2 and Ψ_3 , form a tRNA-shaped structure known as the TSS (22, 49), which serves as a 3' translational enhancer by binding to the P-site of 80S ribosomes through the 60S subunit (35). Upstream of the TSS is hairpin H4, which is important for viral accumulation in protoplasts with undetermined roles in both translation and replication (22, 35, 42). While all carmoviruses have hairpin H5 and Ψ_1 and most have hairpin H4b, only one other carmovirus (*Cardamine chlorotic fleck virus*) has the same series of hairpins and pseudoknots in the 3' UTR as TCV (43). Although the 5' UTR and 3' 400 nt of TCV were synergistic for translational enhancement of a luciferase reporter construct, no canonical or noncanonical long-distance interactions were detected between these two regions (36). However, interactions between 3' sequences and upstream sequences exclusive of the 5' UTR (in addition to the Pr loop long-distance interaction) cannot be ruled out.

Evaluating the effect of disrupting particular elements on surrounding structures has led to the rough mapping of a surprisingly complex network of putative tertiary interactions within the 3' region of TCV (Fig. 1B) (43). These findings led to an initial model whereby the TSS serves as a scaffold for interaction with surrounding elements. These studies also revealed that the Pr loop and H4 internal asymmetric loop (H4AL) play critical roles in virus accumulation and translation as well as in a complex set of regional interactions with each other and with the intervening TSS. For example, altering the Pr loop in an RNA fragment extending from just upstream of H4 to the 3' end structurally affected a residue in the H4 upper stem and three residues in the stem of H4b, as assayed by in-line structure probing (42, 43). Second-site alterations in Pr stem and loop residues were also found in response to primary mutations in H4AL. Mutations in H4AL also affected the structure of the H4 terminal loop (H4TL) (and vice versa), which appeared to control the stability of Ψ_4 (42). These initial studies suggested that a complex network of local interactions may connect many of the elements in the 3' UTR of TCV. The highly interactive nature of TCV 3' elements is also demonstrated by the widespread conformational switch that occurs upon RdRp binding and affects the structure of all these elements (42). This conformational shift, which disrupts the ribosome-binding TSS, was proposed to potentiate the transition between translation and replication when sufficient RdRp had been synthesized.

In this paper, we explore local tertiary interactions in the 3' end of TCV by first identifying residues adjacent to H4 and within the H4TL that, when altered, significantly affect accumulation and translation of the virus. We determined that two highly detrimental mutations reduced accumulation and translation *in vivo* and caused similar structural changes in the Pr loop. Second-site changes that compensate for defects in translation/accumulation were located in selected regions within the 3' UTR (H4, H4b, Pr) as well as in a coding region hairpin and adjacent upstream sequence. All second-site mutations tested reversed the Pr loop structural alterations caused by the initial mutations, suggesting that this specific structural defect correlates with reduced virus viability. The RdRp-mediated conformational shift was found to extend upstream through the coding region hairpin after bypassing much of the intervening USR, supporting a structural connection

between 3' elements and coding region elements. These data are consistent with the Pr loop region, H4b, and H4 being central to the regulation of translation and replication in TCV and allow for the development of an initial map of the higher-order structure of the 3' region of a plus-strand RNA virus.

MATERIALS AND METHODS

Generation of constructs. Oligonucleotide-mediated site-directed mutagenesis was used to generate mutations in full-length TCV using pTCV66, which contains a full-length TCV sequence downstream from a T7 RNA polymerase promoter. All luciferase reporter constructs were generated from T7-Fluc-63-3'UTR, which contains the firefly luciferase open reading frame (ORF) flanked by the TCV 5' UTR (positions 1 to 63) and 3' region (positions 3661 to 4054) (35). PCR fragments (positions 3661 to 4054) containing specific mutants were generated from corresponding TCV full-length mutants and digested with NruI/SpeI or SpeI/SspI. The doubly digested fragments were used to replace the corresponding wild-type (WT) fragments of T7-Fluc-63-3' UTR. All constructs were subjected to regional sequencing to confirm the alterations.

Isolation of second-site mutations. TCV-A3865U and TCV-U3887A were used to generate second-site mutations. Plants (turnip cv. Just Right) at the two-leaf stage were mechanically inoculated with *in vitro*-transcribed RNA (2 μ g for each of two leaves), as described previously (16). Total RNA was extracted at 21 days postinoculation (dpi) from uninoculated upper leaves and then used for reverse transcription (RT)-PCR amplification of fragments corresponding to the 3'-terminal 890 nt of TCV, which were cloned and subjected to sequencing.

Protoplast preparation, inoculation, and RNA gel blots. Protoplasts were prepared using callus cultures from *Arabidopsis thaliana* ecotype Col-0 as previously described (21). To assay for accumulation of TCV, 20 μ g of uncapped, *in vitro*-transcribed TCV gRNA, WT or mutant, was inoculated into protoplasts using 50% polyethylene glycol (PEG) as previously described (21). Total RNA was extracted at 40 h postinoculation (hpi) and subjected to electrophoresis. RNA was transferred to a nitrocellulose membrane, and the gRNA was detected using an [α - 32 P]dCTP random labeled probe corresponding to the 3' 400 nt of TCV. Levels of TCV gRNA were normalized to 26S rRNA.

***In vivo* translation assay.** To assay for translation of the luciferase reporter constructs, 30 μ g of uncapped *in vitro*-transcribed Fluc-containing RNA (WT or mutant) was inoculated into protoplasts using 50% PEG with 10 μ g of uncapped Renilla luciferase (Rluc)-containing transcripts as an internal control as previously described (35). Protoplasts were harvested 18 h later, cells were lysed using passive lysis buffer (Promega), and luciferase activity was detected by a Modulus microplate multimode reader (Turner BioSystems).

***In vitro* RdRp assay.** cDNA for TCV RdRp (p88), together with the in-frame upstream 6 \times His tag coding sequence (CATCACCATCACCAT CAC) and downstream Strep tag II coding sequence (TGGAGCCATCC GCAGTTCGAAAAA), was synthesized by GenScript and cloned into pET-24a(+). RdRp was produced in *Escherichia coli* and purified as described previously (27).

Fragments corresponding to the TCV 3' UTR or TCV 3' 320 nt (positions 3732 to 4054) were synthesized from pTCV66 or pTCV66 mutants using PCR designed to incorporate a T7 RNA polymerase promoter. Transcripts synthesized from the PCR fragments were subjected to *in vitro* RdRp assays using purified recombinant TCV RdRp, as previously described (42).

In-line structural probing. In-line probing was performed as previously described with slight modifications (42, 43). Briefly, TCV 3' UTR or TCV 3' 320-nt (positions 3732 to 4054 nt) transcripts were purified from agarose gels, dephosphorylated with Antarctic phosphatase (NEB), 5'-end labeled using T4 polynucleotide kinase (NEB) and [γ - 32 P]ATP, and then purified by polyacrylamide gel electrophoresis. 5'-End-labeled fragments were denatured at 75°C and slowly cooled to 25°C. RNA (5 pmol) was incubated at 25°C in 50 mM Tris-HCl (pH 8.5) and 20 mM MgCl₂ for

14 h. RdRp used in the in-line probing assays was produced as a fusion with maltose binding protein (MBP) in *E. coli*. In-line probing in the presence of RdRp was carried out by incubating 5 pmol RNA and 7.5 pmol purified MBP-RdRp at 25°C for 1 h, which generated the equivalent level of cleaved products as produced in 14 h in the absence of RdRp (42). RNA cleavage ladders were generated by incubating 5 pmol of end-labeled RNA in 1 µg yeast RNA, 50 mM NaHCO₃-Na₂CO₃ (pH 9.2), and 1 mM EDTA for 5 min at 95°C. RNase T1 digests were produced by incubating 10 pmol of denatured end-labeled RNA in 1 µg yeast RNA, 20 mM sodium citrate (pH 5.0), 1 mM EDTA, 7 M urea, and 1 U RNase T1 (Ambion) for 3 min at room temperature. All reaction mixtures were ethanol precipitated, resuspended with gel loading buffer II (Ambion), heated at 95°C for 2 min, and subjected to electrophoresis through 8 M urea-8% denaturing polyacrylamide gels followed by autoradiography. At least two independent in-line probing assays were produced for each fragment. Profile differences were noted only if found in all replicate gels.

RESULTS

The terminal loop of H4 is important for translation and replication. Our previous studies suggested that a complex network of interactions involving both canonical and noncanonical base pairs connects elements in the 3'UTR of TCV (Fig. 1B) (42, 43). H4AL, which plays a critical role in transcription and translation, was predicted to be an important participant in these interactions, as second-site changes arising in response to H4AL mutations were located throughout the 3' region, including the terminal loop of H4 (H4TL), the stem of H4b, and the Pr apical loop (43). A physical connection between the internal and terminal H4 loops was suggested, as mutations in H4AL altered the structure of H4TL and a 3-nt alteration in H4TL altered the structure of H4AL (42, 43). This H4TL mutation also reduced minus-strand transcription to undetectable levels *in vitro*, suggesting that the H4 apical loop is critical for several important viral processes (42). While these results strongly suggested that H4 is a focal point for interactions that support efficient replication and translation, how this hairpin exerts its effects and whether any interactions extend beyond the artificial boundary of the 3'UTR was not known.

To gain information on the function of H4 and the importance of individual residues within H4TL, single mutations were generated at each H4TL residue in full-length TCV genomic RNA (gRNA) and gRNA transcripts assayed for accumulation at 40 h postinoculation (hpi) of *Arabidopsis thaliana* protoplasts (Fig. 1C). All mutations in H4TL reduced viral gRNA accumulation (Fig. 1D), with alterations between positions 3879 and 3886 causing moderate reductions of between 36% and 69%. In contrast, mutations at U3887 (U3887A or U3887G) severely affected viral accumulation, with mutant gRNA levels reaching only 11% or 6% of the WT level, respectively. Mutations at U3888 were also detrimental for virus accumulation, reducing gRNA accumulation by 75% to 79%.

Viral RNA levels in protoplasts reflect a combination of translation, replication, and stability. To determine whether low accumulation of H4TL mutants is a consequence of defects in translation or replication, two highly detrimental mutations (U3887A and U3887G) and one moderately detrimental mutation (U3886C) were introduced into a reporter construct containing the firefly luciferase (Fluc) ORF flanked by the TCV 5'UTR (positions 1 to 63) and 3' region (positions 3661 to 4054; the 3'UTR starts at position 3801), which together are synergistic for translation (35). U3887A and U3887G reduced expression of the lucifer-

ase construct in *Arabidopsis* protoplasts by 42% and 82%, respectively (Fig. 1E), while U3886C had no effect on luciferase activity. To examine whether these mutations affect transcription by the RdRp, fragments containing the TCV 3'UTR (positions 3801 to 4054) were subjected to *in vitro* RdRp assays using purified, full-length TCV RdRp expressed in *E. coli*. U3886C had a modest effect on minus-strand synthesis, reducing levels by 15%, while U3887G had a more negative effect, reducing transcription to 34% of that of the WT. U3887A produced the opposite effect by enhancing transcription by 2.4-fold (Fig. 1F). These results suggest that while U3887 is a critical nucleotide for H4 function, U3887G and U3887A appear to disrupt different viral processes.

U3887A and U3887G differentially affect the structure of the 3' UTR. U3887G is predicted by Mfold (48) to extend the H4 upper stem and shorten the H4 apical loop through formation of a C-G pair that would also stabilize the adjacent G:U pair (see Fig. 2E). In contrast, U3887A is not predicted to participate in any additional canonical pairing within H4TL. To investigate the validity of these predictions and determine if the alterations lead to any other discernible structural changes within the 3'UTR, mutant and WT fragments were subjected to in-line structure probing, which monitors the flexibility of each residue by assessing the amount of backbone cleavage caused by nucleophilic attack of the 2' hydroxyl group on the backbone phosphate, which requires a flexible base to adopt an "in-line" conformation (31, 39). Fragments were used for this analysis (as opposed to full-length gRNA), as the structure of 3' fragments accurately reflects the structure in the region determined using reverse genetic approaches on full-length gRNA (22). It should be noted, however, that the recent finding of a long-distance interaction between the terminal loop of the Pr hairpin and upstream sequences in the RdRp ORF that is present in a fraction of gRNA transcripts *in vitro* (4) would not be accounted for. Since the TCV 3' region is known to adopt two different conformations (42), cleavage profiles were determined for both the initial conformation of the RNA (Con1) and the RdRp-mediated conformation (Con2).

Fragments containing U3887G exhibited cleavage pattern alterations throughout H4TL in both Con1 and Con2 (Fig. 2A and B). In Con1, cleavages were reduced at positions 3879 to 3884 and 3886 to 3888 and enhanced at position 3885 (Fig. 2A and B, lane 5). These results support the prediction that G3887 pairs with C3880, which reduces the size of H4TL and restricts the flexibility of newly paired nucleotides. In Con2, where the specific conformation of H4 is unknown, cleavages throughout H4TL were reduced (Fig. 2A and B [lane 8] and E). No other cleavage pattern differences were reproducible for U3887G within the 3'UTR. In contrast, U3887A did not alter the flexibility of residues in H4TL with the exception of a slightly reduced intensity of U3883 in Con2 (Fig. 2A and B, lanes 4 and 7). However, U3887A did affect the flexibility of two residues in the Pr loop (positions 4033 and 4034), which were consistently and significantly reduced in Con2 (Fig. 2C [lane 6], D, and F). All together, these results support the hypothesis that U3887G and U3887A affect viral accumulation in different ways.

A single-site alteration upstream of H4 reduces translation, enhances transcription, and causes structural changes in the Pr loop. To determine if the reduced flexibility of Pr loop nucleotides in Con2 might be related to the decreased viability of TCV, we attempted to locate a second residue that, when altered, gives a U3887A-like functional signature (reduced translation, enhanced

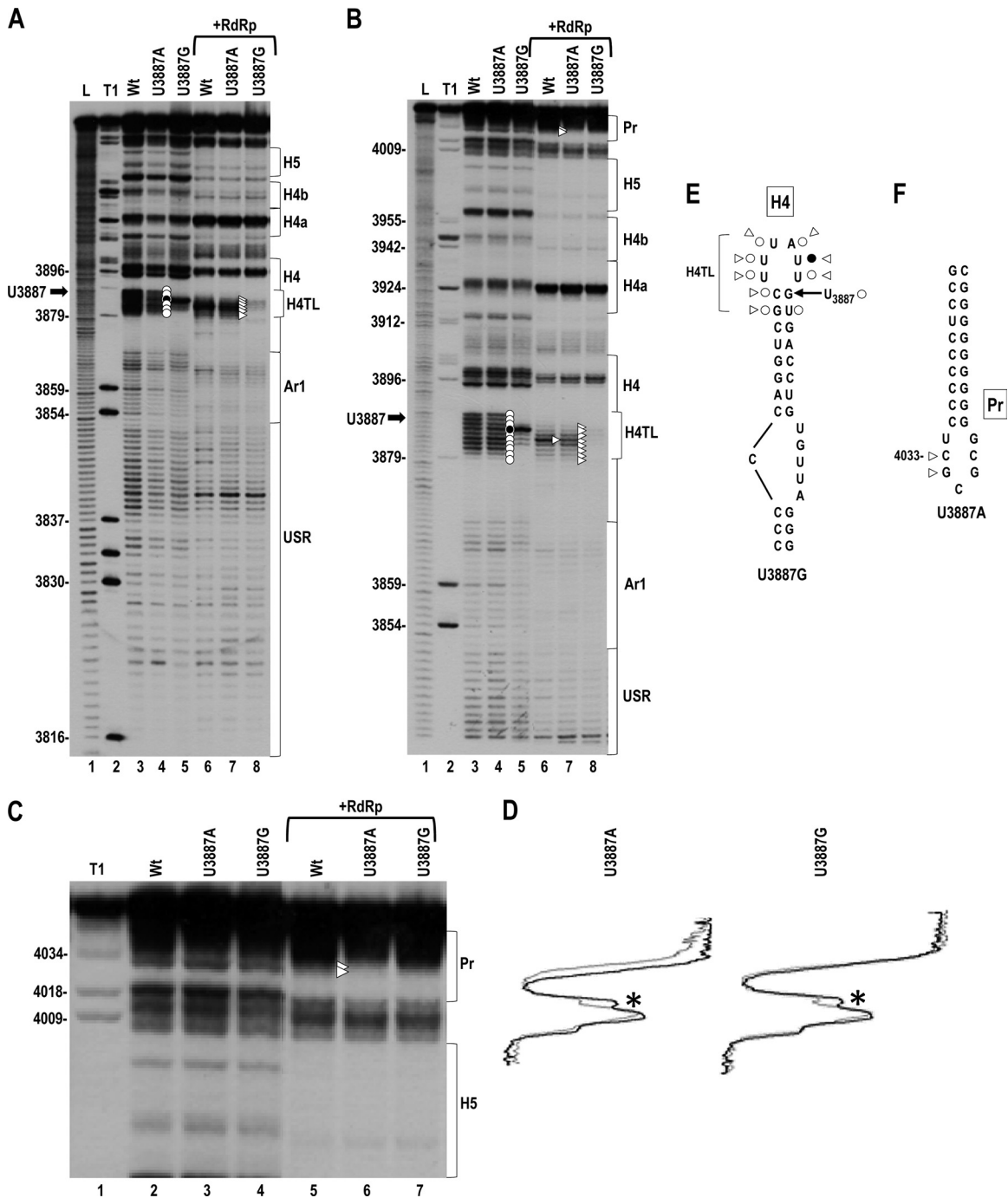


FIG 2 Effect of mutations in H4TL on the structure of the 3'UTR. (A) In-line cleavage of WT 3'UTR transcripts and transcripts containing U3887A or U3887G alterations in the absence or presence of RdRp. Differences between WT and mutants are denoted by circles (in the absence of RdRp) or triangles (in the presence of RdRp). Open and solid circles/triangles denote residues with reduced and increased cleavages, respectively. The thick black arrow denotes mutation sites. L, alkaline hydrolysis ladder; T1, RNase T1 digest (specific for guanylates). In-line cleavage assays were conducted at least twice, and only cleavage pattern differences in all replicates are denoted. (B) Longer run of samples shown in panel A. (C) Enlargement of the upper portion of the autoradiogram in panel B to more clearly show the region from H5 through the Pr. Note that U3887A causes a loss in residue flexibility at positions 4033 and 4034 in the Pr loop in Con2. (D) Densitometry tracing of the autoradiogram in panel C. Black and gray tracings are from Con2 of WT and mutants, respectively. The gap between gray and black corresponds to differences caused by the specific mutations. The asterisk denotes a cleavage difference in the linker between H5 and Pr that is present in the majority of cleavage assays. (E) Residues in H4TL affected by U3887G, which putatively closes the lower portion of the apical loop by pairing with C3880. Symbols are as described in the legend to panel A. (F) Location of residues with altered cleavages in Pr in the presence of RdRp (Con2) in transcripts containing U3887A.

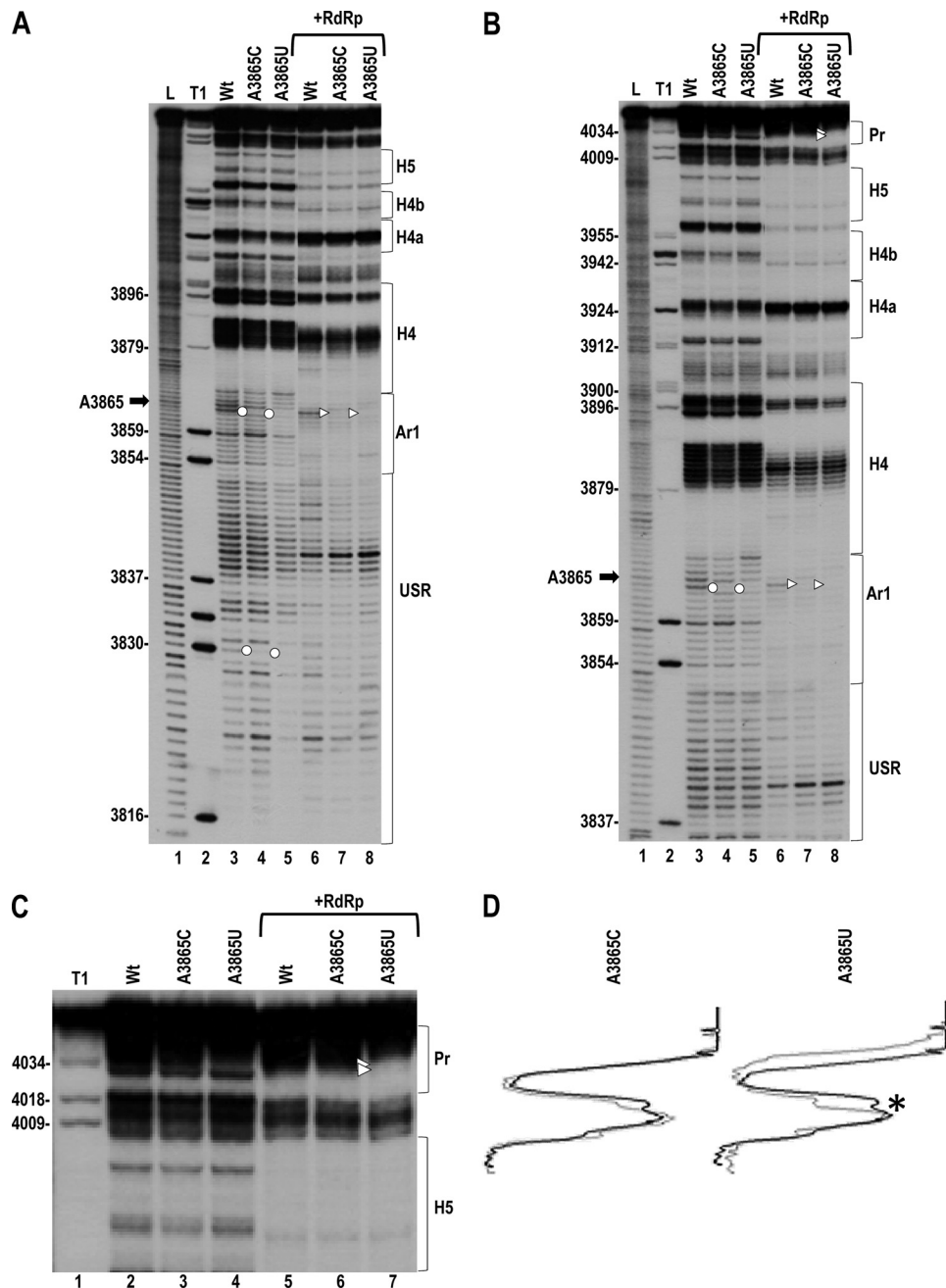


FIG 4 Effect of mutations upstream of H4 on the structure of the 3'UTR. (A) In-line cleavage of WT 3'UTR transcripts and transcripts containing A3865C or A3865U in the absence or presence of RdRp. For details, see the legend to Fig. 2A. The reduced signals near the base of lane 5 were not reproducible. (B) Longer run of samples shown in panel A. (C) Enlargement of the upper portion of the autoradiogram in panel B. Note that A3865U causes a loss in residue flexibility at positions 4033 and 4034 in the Pr loop in Con 2, identical to U3887A (see Fig. 2C). (D) Densitometry tracing of the autoradiograph in panel C. Black and gray tracings are from WT and mutants, respectively, in Con2. The asterisk denotes a cleavage difference in the linker between H5 and Pr that is present in the majority of cleavage assays.

and translation, suggesting that both alterations may be disrupting a similar requirement for virus viability.

A3865U and A3865C were subjected to in-line structure probing to determine how the alterations affected the structure of the 3'UTR fragment. A3865U and A3865C did not alter the cleavage pattern in H4TL, and U3887A did not alter the cleavage in Ar1 (Fig. 2), suggesting that a specific pairing between these two regions is not occurring. Both A3865U and A3865C altered residue

flexibility in their immediate vicinity, with adjacent position 3864 exhibiting reduced flexibility in Con1 and Con2 (Fig. 4A and B, lanes 3, 4, 7, 8). Reduced cleavage was also found for G3830 in both conformations. Furthermore, similar to U3887A, A3865U, but not A3865C, reduced the cleavages at Pr loop residues 4033 and 4034 in Con2 (Fig. 4B [lane 8], C [lane 7], and D). These results suggest that U3887A and A3865U may be causing similar RNA-based disruption of an important viral process that is asso-

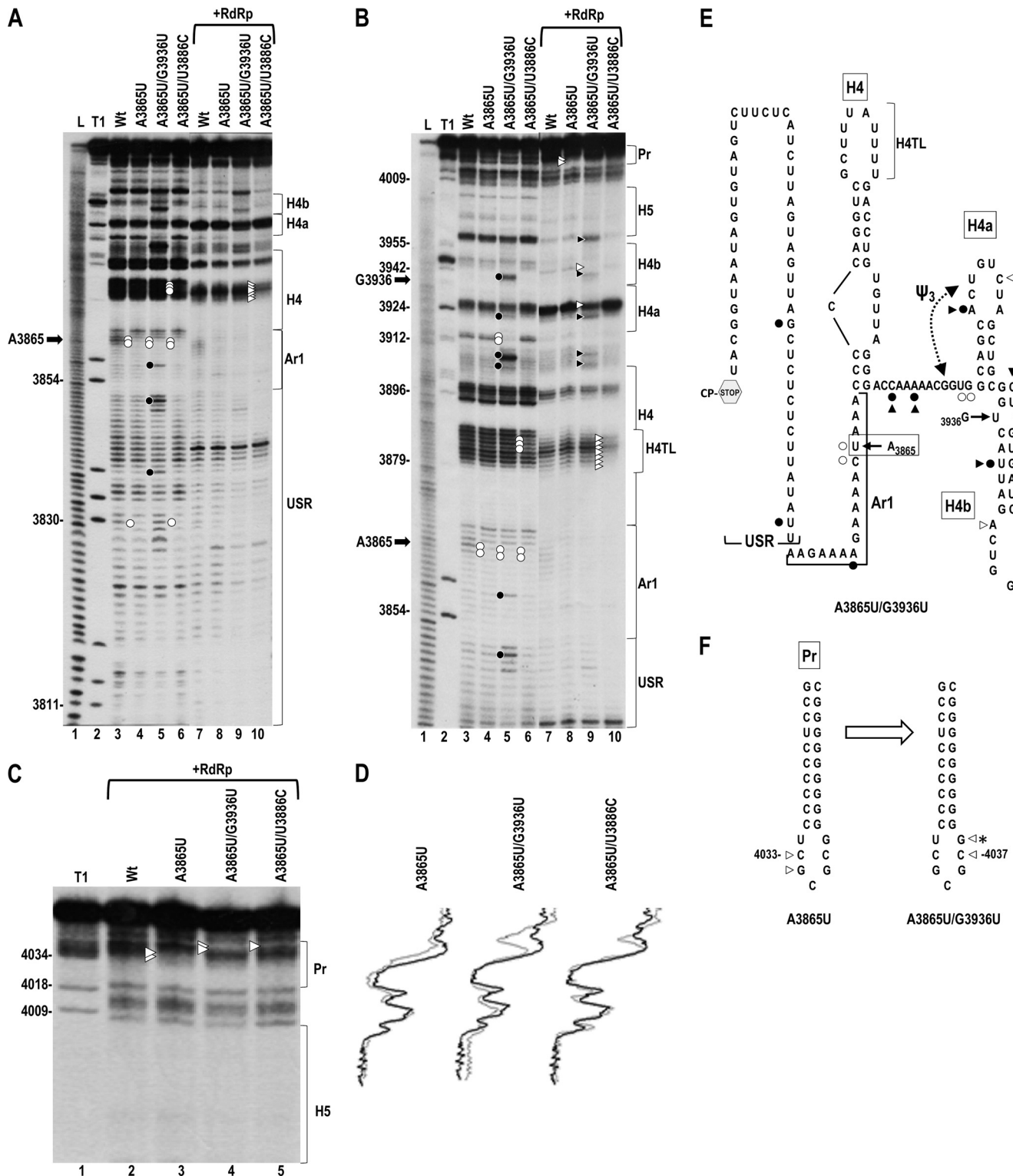


FIG 6 Effect of second-site mutations on the structure of the 3'UTR containing A3865U. (A) In-line cleavage of 3'UTR transcripts with no alterations (WT), A3865U, and A3865U with second-site mutations in the absence or presence of RdRp. See the legend to Fig. 2A for symbol explanations. (B) Longer run of samples shown in panel A. (C) Further extended run of samples in the presence of RdRp to enlarge the Pr region. Note that the combination of A3865U and either of the second-site mutations eliminate the A3865-mediated reduction in residue flexibility at Pr loop positions 4033 and 4034 in the presence of RdRp. (D) Densitometry tracing of the autoradiograph in panel C. See the legend to Fig. 2D. (E) Location of additional cleavage pattern differences in transcripts containing A3865U and second-site mutation G3936U. A3865U is boxed, and the location of G3936U in the stem of hairpin H4b is shown. (F) Location of residues with altered cleavages in Pr in the presence of RdRp in transcripts containing A3865U (left) or A3865U and second-site change G3936U (right). The asterisk denotes the residue with altered cleavage in transcripts containing A3865U and second-site change U3886C.

ciated with restriction in the flexibility of specific Pr loop residues in Con2. As shown in Discussion, Pr loop residue G4034, as well as C4035, G4036, and C4037, were previously shown to be critical for TCW accumulation (43).

Second-site changes associated with A3865U are compensatory for accumulation and translation. If reduced flexibility of Pr loop residues in Con2 correlates with poor viability of TCW containing A3865U or U3887A, then second-site mutations that compensate for the reduced accumulation should restore flexibility of these residues. In addition, if A3865U and U3887A are causing a similar RNA-based disruption of an important TCW function, then the positions of second-site mutations capable of partial or full restoration of function might be similar. To identify second-site mutations arising in the 3' region, WT gRNA and gRNA containing either A3865U or U3887A were inoculated onto turnip plants at the two-leaf stage, and total RNA was isolated 21 days later. Progeny viral RNA derived from both mutant viruses accumulated to levels comparable with that of the WT (Fig. 5A). Sequencing of RT-PCR-generated clones of the 3'-terminal 890 nucleotides revealed that 12/22 progeny of A3865U and 5/18 progeny of U3887A contained second-site changes, and all clones retained the primary mutations. In contrast, the 5'-terminal 1,108 nt from 7 progeny of A3865U and 6 progeny of U3887A did not contain any second-site changes.

Both single and double second-site changes were found for A3865U in individual clones, with locations in the CP ORF (G3767A), USR (U3839C), H4TL (U3886C), stem of H4b (G3936U, G3936A, and G3955A), and Pr stem (C4030U) (Fig. 5B). To determine if one or more of these second-site changes was compensatory, individual or double (if found in the same progeny clone) second-site alterations were incorporated either alone or together with A3865U in full-length gRNA and assayed for effect on virus accumulation in protoplasts. Second-site changes located in the stem of H4b (G3936U/U3839C, G3936U, G3936A/G3955A) and Pr (C4030U) enhanced A3865U viral levels by 5-fold, 14-fold, 55-fold, and 7.6-fold, respectively (Fig. 5C). Two of the second-site changes, U3886C in H4TL and G3767A in the CP ORF (no amino acid change), by themselves reduced viral accumulation by over 50% but together with A3865U accumulated to 76% and 91% of WT levels, respectively (Fig. 5C). To determine if enhanced gRNA accumulation by the second-site changes correlated with enhanced translation, selected second-site changes were incorporated either alone or together with A3865U into the luciferase translation vector. All second-site changes tested enhanced translation of the A3865U-containing transcripts (Fig. 5D). Of the 2 s-site changes that were also assayed for independent effects on translation, H4TL alternation U3886C had no effect, while G3767A alone reduced translation by 54%. Since constructs containing both A3865U and G3767A produced 82% of the WT level of luciferase activity, the two alterations compensated for each other. To determine if the second-site changes affected transcription of A3865U transcripts, 3'UTR-length transcripts (positions 3801 to 4054) containing the primary mutation and 3'UTR-positioned second-site mutations were assayed for minus-strand synthesis. As shown in Fig. 5E, all mutations resulted in levels of minus-strand transcripts that were either similar to the WT level or lower. Since G3767A is located in the CP ORF, extended-length transcripts (positions 3732 to 4054) were used for its transcription assay. Unlike the downstream second-site changes, G3767A enhanced transcription of minus strands (Fig. 5F).

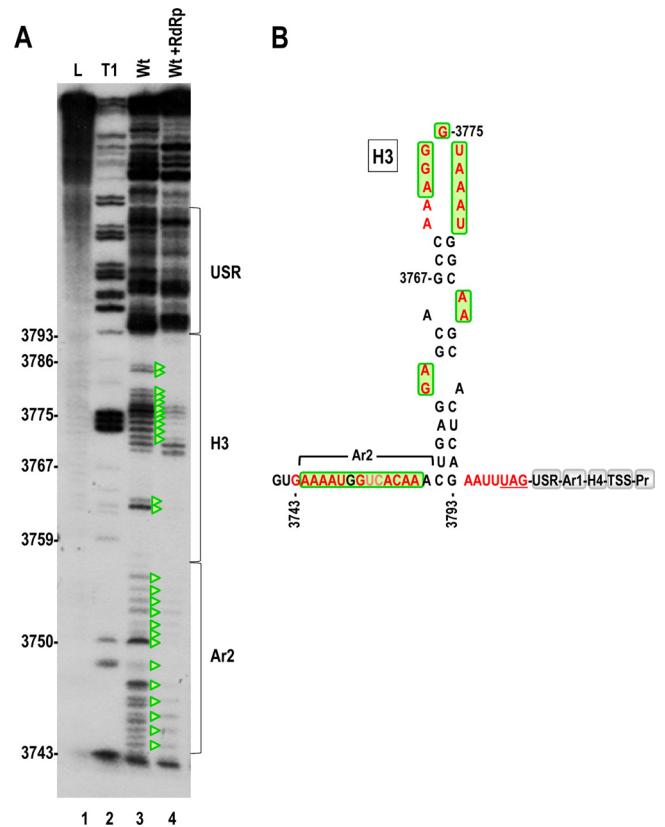


FIG 7 In-line structure probing of the CP ORF 3' region. (A) In-line cleavage of transcripts (positions 3732 to 4054) in the absence or presence of RdRp. Reduction in residue flexibility caused by the RdRp-mediated conformational shift is denoted by green triangles. (B) Location of flexible residues (in red) in the putative secondary structure of hairpin H3 in the CP ORF. Residues boxed in green show reduced flexibility in the presence of the RdRp. Note that residues in the USR have similar cleavage patterns in the presence and absence of RdRp. Ar2, A-rich region just upstream of H3.

Second-site changes G3767A, G3936U, and U3886C reverse the A3865U-mediated structural changes in the Pr loop. To determine if compensatory alterations reverse the A3865U-induced structural changes in the Pr loop, 3'UTR transcripts containing A3865U and downstream second-site mutations G3936U and U3886C were synthesized and subjected to in-line probing (Fig. 6). The presence of H4b stem mutation G3936U caused a number of additional structural changes that were located in (i) the H4b stem, (ii) the apical loop of H4a, (iii) the linker between H4 and H4a, and (iv) the USR in Con1 (Fig. 6A and B [lane 5] and E). In Con2, many of the same cleavage pattern differences were present, with additional changes found in the apical loops of H4a and H4b and in the 3' base of the H4b stem (Fig. 6B [lane 9] and E). In addition, G3936U restored the flexibility of Pr loop residues C4033 and G4034 in Con2, while reducing the flexibility of two other Pr loop residues (Fig. 6C [lane 4] and F). The second-site mutation in H4TL, U3886C, affected cleavages in the H4TL (Fig. 6A and B, lanes 6 and 10) while also restoring the flexibility of Pr loop residues C4033 and G4034 in Con2 and causing the loss of flexibility of one other Pr loop residue (Fig. 6C, lane 5). Neither second-site change affected the residues in the USR or Ar1, whose cleavage pattern was altered by A3865U.

Since second-site alteration G3767A supported near-WT levels

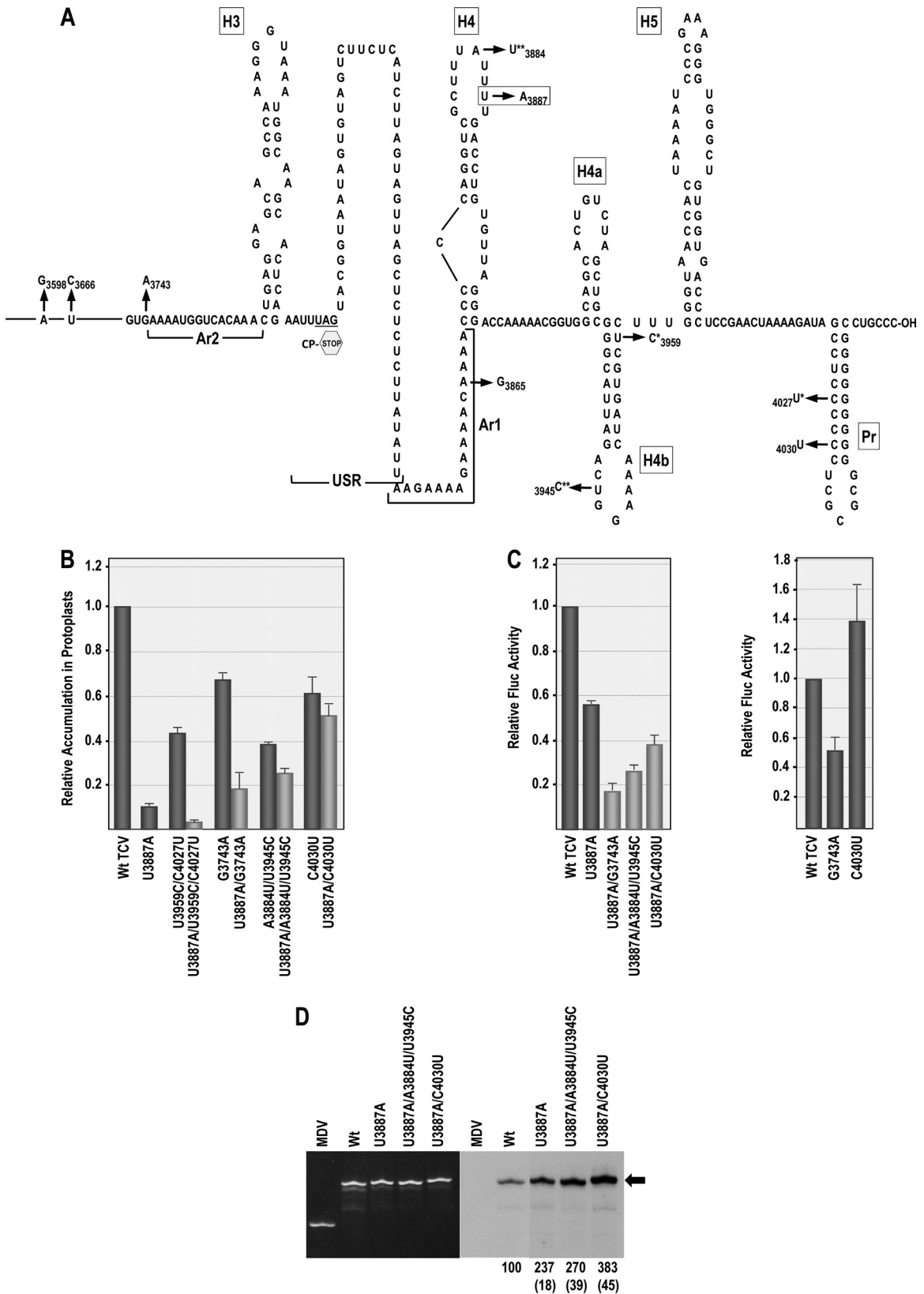


FIG 9 Second-site changes associated with primary mutation U3887A. (A) Location of second-site changes associated with U3887A in the 3'UTR and nearby CP ORF. Primary mutation U3887A is boxed. Second-site changes labeled with asterisks denote that they were found in the same clone. (B) Effect of second-site mutations on accumulation of U3887A transcripts in protoplasts at 40 hpi. Gray bars denote accumulation of second-site mutations combined with U3887A. Average values from three experiments and standard deviations are shown. (C) Effect of second-site mutations on translation of luciferase transcripts containing

of accumulation and translation in conjunction with A3865U, it was also tested for effect on the flexibility of Pr loop residues when combined with A3865U. The location of G3767 in the CP ORF required that in-line cleavage patterns for Con1 and Con2 be established for an extended 3' fragment (positions 3732 to 4054). In-line structure probing of the extended fragment supported positioning G3767 in a hairpin (H3) just upstream of the CP stop codon, which had previously been identified as a nucleation site for CP binding and capsid assembly (25) (Fig. 7A [lane 3] and B). The presence of the RdRp caused a substantial conformational shift in H3 that did not extend downstream into the USR, with most H3 residues losing flexibility. The presence of 69 additional residues in the extended 3' fragment did not discernibly affect the cleavage pattern in the 3'UTR in either conformation (Fig. 8 and data not shown). These results suggest a structural connection between H3 and the 3' proximal elements that undergo an extensive conformational shift in the presence of the RdRp.

In the extended fragment, A3865U altered the structure of the same residues previously found for the 3'UTR fragment, including Pr loop residues C4033 and G4034 in Con2 (Fig. 8). In addition, A3865U was responsible for enhanced cleavage of one residue in the apical loop of H3 (U3776) and one residue upstream of H3 in an A-rich region (Ar2) within a motif identical to that in the vicinity of A3865 (3753ACAAA [underlined residue exhibited the enhanced flexibility]). G3767A alone impacted the structure of H3 in both conformations, as well as USR residues between positions 3846 and 3851 in Con2 (Fig. 8A, B, and C [lanes 5 and 9] and F). In addition, G3767A combined with A3865U restored the flexibility of Pr loop residues C4033 and G4034 and most structural differences in the USR due to A3865U (Fig. 8B and C [lane 6 and 10], D [lane 5], and E). These results indicate that all second-site mutations tested were both compensatory to various extents for the presence of A3865U and restored Pr loop residues C4033 and G4034 to the WT cleavage pattern. This suggests that the altered cleavage pattern in the Pr loop may be a signpost for the negative effect on accumulation and translation of A3865U.

Compensatory second-site changes associated with U3887A partially restore the structural changes in the Pr loop. Second-site changes for U3887A were located at three positions within the CP ORF (A3598G, U3666C, and G3743A), just upstream of H4 (A3865G), in H4TL (A3884U), in H4b (loop residue U3945C and stem residue U3959C), and two positions in the Pr stem (C4027U, C4030U). These second-site mutations are positioned very similarly as those for A3865U, with one (in the Pr stem) being an identical alteration (C4030U) and one being at position 3865 (Fig. 9A).

gRNA containing individual or double second-site changes alone accumulated to 38 to 68% of that of the WT (Fig. 9B). Three of the four single or multiple (if found in the same clone) second-site mutations (G3743A in the CP ORF [no amino acid change], A3884U/U3945C, and C4030U) compensated for U3887A, with viral levels enhanced by 1.7-, 2.3-, and 4.6-fold, respectively (Fig. 9B). Unlike A3865U, none of the second-site changes compensated for the moderately reduced translation of U3887A (Fig. 9C, left), and the 2 s-site changes tested enhanced minus-strand tran-

scription (Fig. 9D). These results suggest that while most second-site mutations are compensatory in full-length gRNA, there is no correlation with improvement of any specific viral process using the current assays.

To determine if the second-site changes associated with U3887A restored the U3887A-induced structural alterations in the Pr loop, transcripts containing individual (C4030U) or double (A3884U and U3945C) second-site changes together with U3887A were subjected to in-line probing. Both additions restored the WT cleavage pattern of the Pr loop (Fig. 10). In addition, the presence of second-site mutations A3884U and U3945C caused slight structural changes in the local regions of the mutations (Fig. 10A and B [lane 6] and B [lane 10]). All together, these data revealed that second-site changes that compensated to various extents for the reduced viral accumulation due to A3865U and U3887A *in vivo* restored the flexibility of Pr loop residues C4033 and G4034 in Con2 *in vitro*.

DISCUSSION

The dynamic nature of RNA permits fundamental processes to be controlled by conformational changes triggered by alterations in the local concentration of interacting factors (13, 29). Understanding how RNA viruses make use of their genome's inherent plasticity to switch between incompatible activities, such as translation and replication or package into the tight confines of an icosahedra capsid, is complicated by the complexity of the RNA structural landscape that maximizes hydrogen bonds involving all three edges of a nitrogenous base (17, 32). RNA folding involves multiple levels of interactions with simple secondary structural helices that coaxially align and interact locally and distally through canonical and noncanonical pairings to concentrate the RNA into a globular three-dimensional (3-D) form (11, 33). Some, but not all, plus-strand RNA viruses contain a substantial number of genome-wide secondary structure elements (genome-scale ordered RNA structure [GORS]) and adopt a compact spheroid shape that correlates with viral persistence (5, 6). While RNA viruses likely make extensive use of local and long-distance RNA interactions between such secondary structure elements to control basic processes, only a limited number of such interactions have been reported, with identified connections forming more readily discernible canonical base pairings (3, 4, 9, 10, 12, 13, 14, 15, 23, 26, 28, 40, 41).

Our previous studies identified a tRNA-like 3-D structure within the 3'UTR of TCV that is composed of three hairpins and two pseudoknots and serves as a scaffold for additional interactions in the region (22, 35, 42). While the ribosome-binding properties of the TSS correlate with translational efficiency, alterations within the internal and apical loops of the adjacent upstream hairpin H4 also significantly affected replication and translation. A central role for H4 within the structure of the 3' region was suggested by the location of both second-site changes that compensate for mutations within H4AL and structural changes arising from these mutations (43). While these studies suggested that elements within the 3'UTR of TCV might be intimately connected through a network of canonical and noncanonical interactions, the extent of such a network was not known.

U3887A in protoplasts. See the legend to Fig. 1E. Left, effect on translation of luciferase transcripts containing U3887A combined with selected second-site mutations; right, effect on translation of selected second-site mutations alone. (D) *In vitro* transcription of WT and mutant 3'UTR fragments (positions 3801 to 4054) using purified recombinant RdRp. The EtBr-stained gel is at the left, and the corresponding autoradiogram is at the right. See the legend to Fig. 1F.

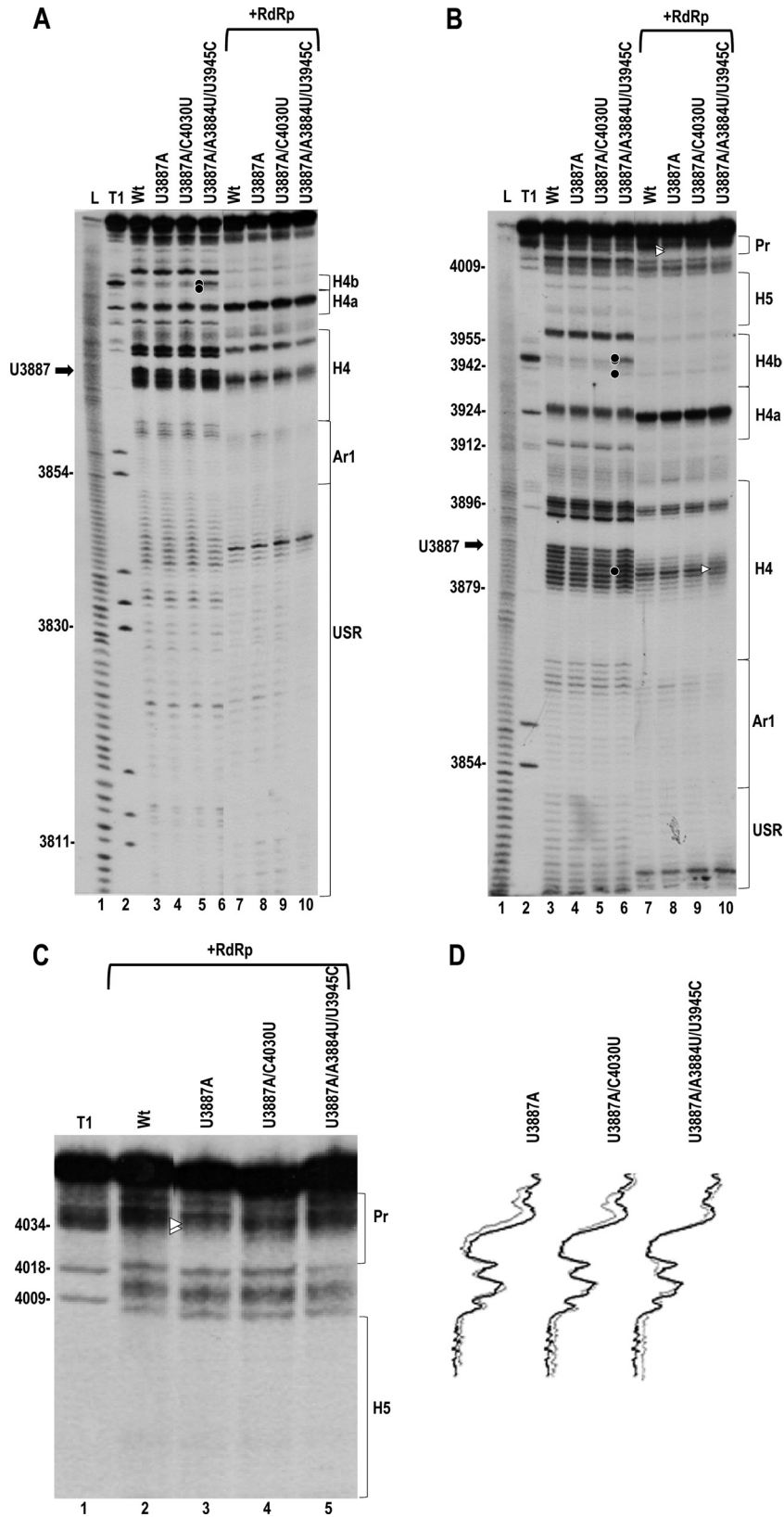


FIG 10 Effect of second-site mutations on the structure of the 3'UTR containing U3887A. (A) In-line cleavage of 3'UTR transcripts with no alterations (WT), U3887A, and U3887A with second-site mutations in the absence or presence of RdRp. See the legend to Fig. 2A for symbol explanations. (B) Longer run of samples shown in panel A. (C) Further extended run of samples in the presence of RdRp to enlarge the Pr region. Note that the combination of U3887A and either of the second-site mutations eliminates the U3887A-mediated reduction in residue flexibility at Pr loop positions 4033 and 4034. (D) Densitometry tracing of the autoradiograph in panel C. See the legend to Fig. 2D.

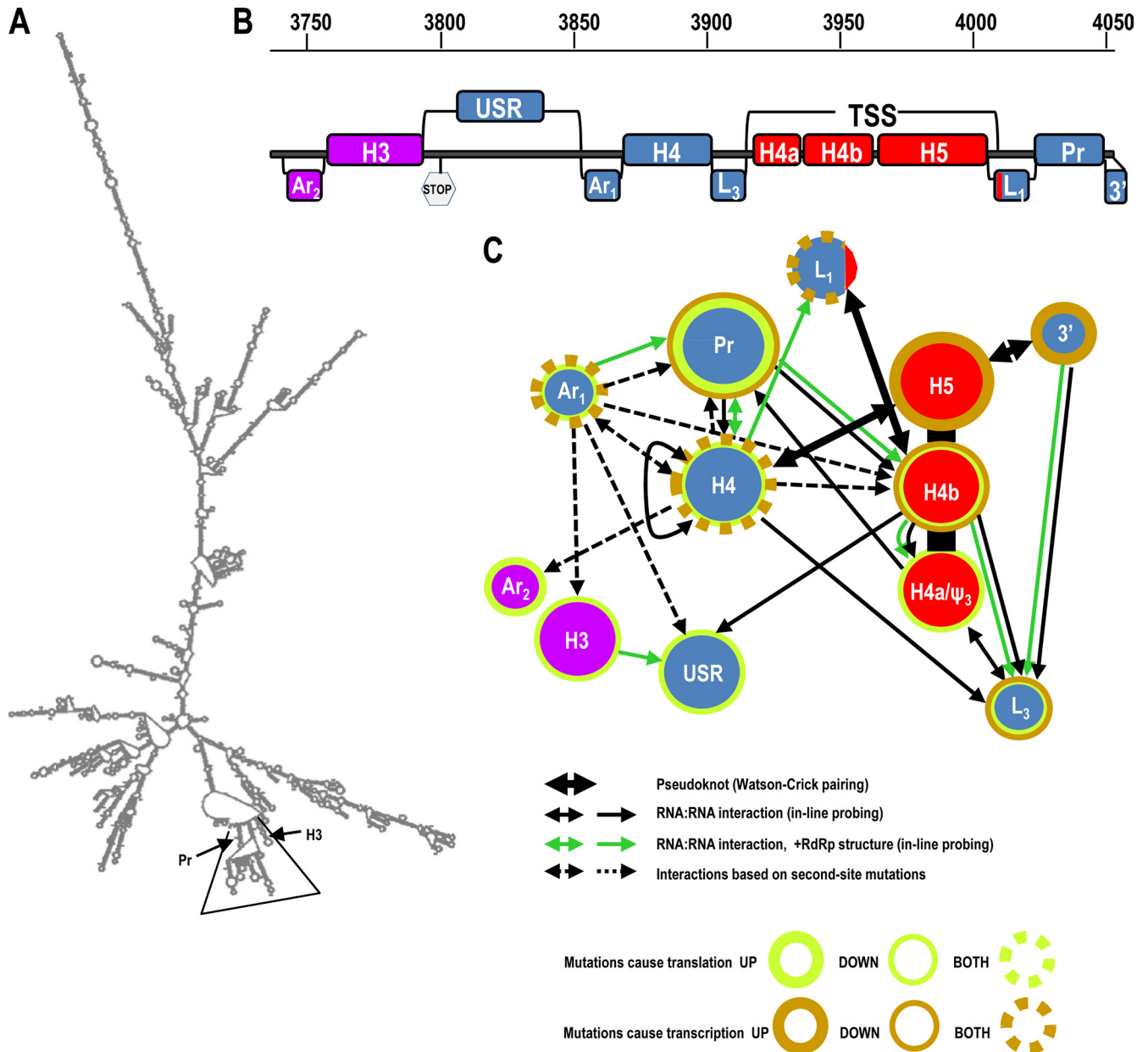


FIG 11 Interactome in the 3' region of TCV. (A) Mfold secondary structure prediction for full-length TCV genomic RNA. The domain containing the 3' hairpins from H3 through Pr is enclosed. Locations of Pr and H3 are shown. (B) Relative positions of particular elements in the 3' region of TCV. Elements in the CP ORF are colored purple, and elements that form the TSS are colored red. TSS, tRNA-shaped structure; L, linker; Ar1, A-rich region just upstream of H4; Ar2, A-rich region just upstream of H3; USR, largely unstructured region. (C) Network of putative tertiary interactions that connect elements in the TCV 3' region. Elements are colored as described in the legend to panel A. Circular bands reflect the effect of mutations on translation (green) or transcription (brown). Thick and thin bands denote that disruption of elements enhances or reduces translation/transcription, respectively. Broken bands indicate that mutations within the element can have opposite effects on translation/transcription. Putative tertiary interactions are denoted by arrows. Thick double-headed arrows denote pseudoknots, which were mapped genetically. Black and green thin lines denote that disruption of one element affects the structure of the element the line points to in the initial conformation and the RdRp-mediated conformation, respectively. Dashed arrows indicate that mutations in one element generate second-site changes in the other. Bidirectional arrows reflect reciprocal effect. (D) Location of H4b (blue) in the structure of the TSS.

For this report, we investigated local tertiary interactions in the 3' end of TCV by identifying deleterious mutations in two previously poorly explored regions: H4TL and the A-rich region just upstream of H4 (Ar1). While both mutations (U3887A and A3865U) had similar effects on some viral processes (reduced translation and accumulation), A3865U appeared to have at most a slight positive effect on minus-strand synthesis *in vitro*, whereas

U3887A enhanced minus-strand synthesis by 2.4-fold. As has been previously noted, enhanced transcription of minus strands in the TCV system does not necessarily correlate with enhanced accumulation in protoplasts and plants, since accumulation in cells is likely dependent on precise levels of conformers that promote replication, translation, and other cellular activities (42, 45). Both U3887A and A3865U also substantially reduced the flexibil-

ity of Pr loop residues C4033 and G4034 in Con2, suggesting that this structural alteration may reflect a common signature for disrupting a required conformation. Alterations at adjacent residues (or even the same residue) had either limited effects or very different effects on viral processes (Fig. 1 and 3) and were not associated with structural alterations in the Pr loop (Fig. 2 and 4). We therefore propose that U3887A and A3865U have a base-specific, added ability to disrupt the conformation of the 3' region rather than simply disrupting a residue needed for direct binding (to H4 or Ar1) of a host or viral factor. Although common structural alterations are discernible only for the RdRp-mediated Con2 conformation, both mutations reduced translation of the luciferase reporter constructs, suggesting that the mutations affect more than the conformational switch. However, we cannot rule out the possibility that both alterations similarly affect binding of a required element to a locally disrupted structure.

We reasoned that if A3865U and U3887A were similarly capable of disrupting the global conformation of the 3' region, then second-site mutations that restored a more functional structure might not be restricted to any particular element but might be found in similar locations throughout the 3' region. Both A3865U in Ar1 and U3887A in H4TL generated second-site changes in each other's local region, as well as in the Pr stem, H4b stem, and a region near the end of the CP ORF (Fig. 5 and 9). For A3865U, all second-site alterations tested compensated to various extents for defects in accumulation, and all tested alterations reversed the structural alteration in the Pr loop in Con2. The second-site mutations tested for U3887A also were compensatory to various extents for accumulation and reversed the Pr loop structural defect. However, there was no compensation for the reduction in translation associated with U3887A (Fig. 9C). This could reflect that restoration of a different viral process enhances accumulation despite further reductions in translation.

Our finding that U3887A and A3865U correlate with a specific structural defect in the Pr loop is consistent with previous results indicating that the Pr loop is critical for accumulation of TCV. Alterations of individual residues in 4034GCGC reduced TCV gRNA to near undetectable levels, while mutations in other residues in the Pr loop had only a limited effect on accumulation (43). The structure of the Pr loop was also altered by disruptions in Ψ_3 and H4AL, while mutations in the Pr loop affected the structure of the H4b stem and the stem of H4 (42, 43). The recent finding that the Pr loop is engaged in a long-distance RNA-RNA interaction that promotes ribosomal readthrough translation of the RdRp (4) suggests a possible mechanism whereby mutations that alter the conformation of Pr loop residues could affect (either positively or negatively) the production of the RdRp.

Second-site alteration G3936U located in the H4b stem caused structural changes in the USR, linker between H4 and the TSS (L3), H4a/ Ψ_3 , as well as local structural changes in H4b (Fig. 6). The structural connection between H4a/ Ψ_3 and H4b correlate with our previous report that the region from Ψ_3 through H4b of TCV and *satC* can be functionally replaced by the analogous region of the related virus *Cardamine chlorotic fleck virus* (CCFV) but not by the individual hairpins (22, 44).

Several second-site changes were located upstream of the USR within the CP ORF, suggesting that the interacting network extends considerably further than previously thought. G3767A, located in a hairpin (H3) previously identified as a nucleation site for packaging by the TCV CP when associated with a heterologous

viral RNA (25), was able to restore close to WT levels of accumulation and translation when combined with A3865U. Second-site changes in this region were also associated with primary mutations in H4AL (43). A structural connection between the H3 region and downstream elements that bypasses the intervening USR is also implied by finding that the RdRp-mediated conformational shift extends into this region (Fig. 7) but only slightly changes residues in the USR. In addition, A3865U alters the structure of several residues in the H3 region, and G3767A alters the structure of residues in and near Ar1 (Fig. 8). An intriguing possibility is that participation of the H3 packaging site in an interactive network of RNA elements shields the site from packaging prior to the cessation of replication and translation activities. Whether additional regions further upstream participate in this interactive network is not yet known.

Twenty-nine of the 39 lowest free energy structures for TCV genomic RNA predicted by Mfold contain hairpins H3 through Pr in a separate domain that extends off a central folded "spine" (Fig. 11A), which is phylogenetically conserved in the most closely related carmovirus (CCFV; 65% conserved). Figure 11B and C presents an RNA interactome delineating connections within this domain that takes into account the location of compensatory mutations and structural alterations visualized by in-line probing. Based on our current results, hairpins H4, H4b, and Pr play central roles among these interactions. Mutations in different elements also have distinctive effects on replication and translation, illustrated by bands that encircle the elements. For example, all mutations (that affect viral accumulation) in the Pr enhance translation and reduce transcription, whereas all mutations in H4b reduce translation and transcription. Mutations in H4a and the upstream Ar1 region all reduce translation, but different mutations can have opposing effects on transcription. While the pseudoknots (thick connecting lines) connect sequences by canonical Watson-Crick base pairing, the remaining connections are likely the result of a combination of canonical and noncanonical interactions. This work illustrates the complex interactions necessary for expression and replication of a multifunctional viral RNA genome and the need to consider the higher-order 3-D structure of the RNA when interpreting results derived from reverse genetic studies.

ACKNOWLEDGMENT

This work was supported by a grant from the U.S. Public Health Service (GM 061515-05A2/G120CD) to A.E.S.

REFERENCES

- Ahlquist P. 2006. Parallels among positive-strand RNA viruses, reverse-transcribing viruses and double-stranded RNA viruses. *Nature Rev. Microbiol.* 4:371–382.
- Reference deleted.
- Chattopadhyay M, Shi K, Yuan X, Simon AE. 2011. Long-distance kissing loop interactions between a 3' proximal Y-shaped structure and apical loops of 5' hairpins enhance translation of Saguaro cactus virus. *Virology* 417:113–125.
- Cimino PA, Nicholson BL, Wu B, Xu W, White KA. 2011. Multifaceted regulation of translational readthrough by RNA replication elements in a Tombusvirus. *PLoS Path* 7:e1002423.
- Davis JH, et al. 2005. RNA helical packing in solution: NMR structure of a 30 kDa GAAA tetraloop-receptor complex. *J. Mol. Biol.* 351:371–382.
- Davis M, Sagan SM, Pezacki JP, Evans DJ, Simmonds P. 2008. Bioinformatic and physical characterizations of genome-scale ordered RNA structure in mammalian RNA viruses. *J. Virol.* 82:11824–11836.
- Doudna JA, Sarnow P. 2007. Translation initiation by viral internal ribo-

- some entry sites, p 129–154. *In* Mathews NSM, Hershey JWB (ed), Translational control in biology and medicine. Cold Spring Harbor Laboratory Press, Cold Spring Harbor, NY.
8. Dreher TW, Miller WA. 2006. Translational control in positive strand RNA plant viruses. *Virology* 344:185–197.
 9. Edgil D, Harris E. 2006. End-to-end communication in the modulation of translation by mammalian RNA viruses. *Virus Res.* 119:43–51.
 10. Fabian MR, White KA. 2006. Analysis of a 3'-translation enhancer in a tombusvirus: a dynamic model for RNA-RNA interactions of mRNA termini. *RNA* 12:1304–1314.
 11. Hermann T, Patel DJ. 1999. Stitching together RNA tertiary architectures. *J. Mol. Biol.* 294:829–849.
 12. Hu B, Pillai-Nair N, Hemenway C. 2007. Long-distance RNA-RNA interactions between terminal elements and the same subset of internal elements on the potato virus X genome mediate minus- and plus-strand RNA synthesis. *RNA* 13:267–280.
 13. Iglesias NG, Gamarnik AV. 2011. Dynamic RNA structures in the dengue virus genome. *RNA Biol.* 8:249–257.
 14. Jiwan SD, White KA. 2011. Subgenomic mRNA transcription in Tombusviridae. *RNA Biol.* 8:287–294.
 15. Karetnikov A, Lehto K. 2008. Translation mechanisms involving long-distance base pairing interactions between the 5' and 3' non-translated regions and internal ribosomal entry are conserved for both genomic RNAs of Blackcurrant reversion nepovirus. *Virology* 371:292–308.
 16. Kong QZ, Wang JL, Simon AE. 1997. Satellite RNA-mediated resistance to turnip crinkle virus in Arabidopsis involves a reduction in virus movement. *Plant Cell* 9:2051–2063.
 17. Leontis NB, Stombaugh J, Westhof E. 2002. The non-Watson-Crick base pairs and their associated isostericity matrices. *Nucleic Acids Res.* 30:3497–3531.
 18. Leontis NB, Westhof E. 2001. Geometric nomenclature and classification of RNA base pairs. *RNA* 7:499–512.
 19. Li Z, Nagy PD. 2011. Diverse roles of host RNA-binding proteins in RNA virus replication. *RNA Biol.* 8:305–315.
 20. Lin HX, White KA. 2004. A complex network of RNA-RNA interactions controls subgenomic mRNA transcription in a tombusvirus. *EMBO J.* 23:3365–3374.
 21. McCormack JC, Simon AE. 2005. Callus cultures of Arabidopsis. *Curr. Protoc. Microbiol.* 16:Unit 16D.1.
 22. McCormack JC, et al. 2008. Structural domains within the 3' untranslated region of turnip crinkle virus. *J. Virol.* 82:8706–8720.
 23. Miller WA, White KA. 2006. Long-distance RNA-RNA interactions in plant virus gene expression and replication. *Annu. Rev. Phytopath.* 44:447–467.
 24. Qu F, Morris TJ. 2000. Cap-independent translational enhancement of turnip crinkle virus genomic and subgenomic RNAs. *J. Virol.* 74:1085–1093.
 25. Qu F, Morris TJ. 1997. Encapsidation of turnip crinkle virus is defined by a specific packaging signal and RNA size. *J. Virol.* 71:1428–1435.
 26. Romero-Lopez C, Berzal-Herranz A. 2009. A long-range RNA-RNA interaction between the 5' and 3' ends of the HCV genome. *RNA* 15:1740–1752.
 27. Schmidt TGM, Skerra A. 2007. The Strep-tag system for one-step purification and high-affinity detection or capturing of proteins. *Nat. Protoc.* 2:1528–1535.
 28. Serrano P, Pulido MR, Saiz M, Martinez-Salas E. 2006. The 3' end of the foot-and-mouth disease virus genome establishes two distinct long-range RNA-RNA interactions with the 5' end region. *J. Gen. Virol.* 87:3013–3022.
 29. Simon AE, Gehrke L. 2009. RNA conformational changes in the life cycles of RNA viruses, viroids, and virus-associated RNAs. *Biochim. Biophys. Acta-Gene Reg. Mech.* 1789:571–583.
 30. Song CZ, Simon AE. 1995. Requirement of a 3'-terminal stem-loop in *in vitro* transcription by an RNA-dependent RNA-polymerase. *J. Mol. Biol.* 254:6–14.
 31. Soukup GA, Breaker RR. 1999. Relationship between internucleotide linkage geometry and the stability of RNA. *RNA* 5:1308–1325.
 32. Stombaugh J, Zirbel CL, Westhof E, Leontis NB. 2009. Frequency and isostericity of RNA base pairs. *Nucleic Acids Res.* 37:2294–2312.
 33. Strobel SA, Doudna JA. 1997. RNA seeing double: close-packing of helices in RNA tertiary structure. *Trends Biochem. Sci.* 22:262–266.
 34. Reference deleted.
 35. Stupina VA, et al. 2008. The 3' proximal translational enhancer of Turnip crinkle virus binds to 60S ribosomal subunits. *RNA* 14:2379–2393.
 36. Stupina VA, Yuan X, Meskauskas A, Dinman JD, Simon AE. 2011. Ribosome binding to a 5' translational enhancer is altered in the presence of the 3'UTR in *cap*-independent translation of turnip crinkle virus. *J. Virol.* 85:4638–4653.
 37. Sun XP, Simon AE. 2006. A *cis*-replication element functions in both orientations to enhance replication of turnip crinkle virus. *Virology* 352:39–51.
 38. Villordo SM, Alvarez DE, Gamarnik AV. 2010. A balance between circular and linear forms of the dengue virus genome is crucial for viral replication. *RNA* 16:2325–2335.
 39. Winkler WC, Cohen-Chalamish S, Breaker RR. 2002. An mRNA structure that controls gene expression by binding FMN. *Proc. Natl. Acad. Sci. U. S. A.* 99:15908–15913.
 40. Wu B, et al. 2009. A discontinuous RNA platform mediates RNA virus replication: building an integrated model for RNA-based regulation of viral processes. *PLoS Pathog.* 5:e1000323.
 41. You S, Padmanabhan R. 1999. A novel *in vitro* replication system for dengue virus—initiation of RNA synthesis at the 3' end of exogenous viral RNA templates requires 5' and 3'-terminal complementary sequence motifs of the viral RNA. *J. Biol. Chem.* 274:33714–33722.
 42. Yuan XF, Shi KR, Meskauskas A, Simon AE. 2009. The 3' end of turnip crinkle virus contains a highly interactive structure including a translational enhancer that is disrupted by binding to the RNA-dependent RNA polymerase. *RNA* 15:1849–1864.
 43. Yuan XF, Shi KR, Young MYL, Simon AE. 2010. The terminal loop of a 3' proximal hairpin plays a critical role in replication and the structure of the 3' region of turnip crinkle virus. *Virology* 402:271–280.
 44. Zhang GH, Zhang JC, George AT, Baumstark T, Simon AE. 2006. Conformational changes involved in initiation of minus-strand synthesis of a virus-associated RNA. *RNA* 12:147–162.
 45. Zhang GH, Zhang JC, Simon AE. 2004. Repression and derepression of minus-strand synthesis in a plus-strand RNA virus replicon. *J. Virol.* 78:7619–7633.
 46. Reference deleted.
 47. Zhong X, et al. 2006. Tertiary structural and functional analyses of a viroid RNA motif by isostericity matrix and mutagenesis reveal its essential role in replication. *J. Virol.* 80:8566–8581.
 48. Zuker M. 2003. Mfold Web server for nucleic acid folding and hybridization prediction. *Nucleic Acids Res.* 31:3406–3415.
 49. Zuo XB, et al. 2010. Solution structure of the *cap*-independent translational enhancer and ribosome-binding element in the 3' UTR of turnip crinkle virus. *Proc. Natl. Acad. Sci. U. S. A.* 107:1385–1390.